Applied Physics
Express

LETTER • **OPEN ACCESS**

Epitaxial film growth of strongly correlated $LaNiO_3$ on buffered Si and thermal conductivity modulation based on reversible protonation

To cite this article: Haruka Zaizen *et al* 2026 *Appl. Phys. Express* **19** 031006

OPEN ACCESS

Applied Physics Express 19, 031006 (2026) LETTER

https://doi.org/10.35848/1882-0786/ae49e1

Epitaxial film growth of strongly correlated $LaNiO_3$ on buffered Si and thermal conductivity modulation based on reversible protonation

Haruka Zaizen[1], Hao-Bo Li[1,2*], Osamu Nakagawara[3], Saeko Tonda[1], Ahrong Jeong[4], Hiromichi Ohta[4], and Hidekazu Tanaka[1,2*]

[1]SANKEN, The University of Osaka, Ibaraki, Osaka 567-0047, Japan
[2]Spintronics Research Network Division, Institute for Open and Transdisciplinary Research Initiatives, The University of Osaka, Yamadaoka 2-1, Suita, Osaka 565-0871, Japan
[3]I-PEX Piezo Solutions Inc. Yamaguchi 755-0152, Japan
[4]Research Institute for Electronic Science, Hokkaido University, N20W10, Sapporo 001-0020, Japan

*E-mail: h.b.li.phys@sanken.osaka-u.ac.jp; h-tanaka@sanken.osaka-u.ac.jp

Received January 23, 2026; revised February 19, 2026; accepted February 24, 2026; published online March 19, 2026

Toward a high-efficiency energy harvesting device, such as a thermal transistor, thermal conductivity modulation based on strongly correlated oxides is proposed and explored. High-quality epitaxial film growth of strongly correlated oxides on large-area Si substrates is essential to match industrial needs. In this work, $LaNiO_3$ thin films are epitaxially grown on buffer-layer-coated Si(001) substrates. Reversible protonation of the $LaNiO_3$ thin film via ionic liquid gating achieves thermal conductivity modulation in the range of 0.9 to 3.0 W m^{-1} K^{-1} and is comparable to that of a prototype laboratory device on a single crystal substrate. © 2026 The Author(s). Published on behalf of The Japan Society of Applied Physics by IOP Publishing Ltd

Supplementary material for this article is available online

Strongly correlated materials are known to exhibit emergent properties, such as high-temperature superconductivity and multiferroics, due to the strong interaction between different degrees of freedom.[1–3] Among all the strongly correlated oxides, transition metal perovskite *RE*NiO_3 (*RE* = rare-Earth elements) has been investigated for decades as typical Mott insulators with intrinsic metal–insulator transition (MIT).[4,5] Especially, the near-room-temperature transition temperature (e.g. $NdNiO_3$ ~200 K; $SmNiO_3$ ~400 K) would benefit the solution of next-generation electronic devices towards the "Beyond CMOS" strategy.[6,7] Recently, by inserting a proton into *RE*NiO_3, another type of MIT has been observed in $SmNiO_3$ and $NdNiO_3$.[7] Unlike the intrinsic MIT described, the MIT induced by proton injection fundamentally stems from the B-site element reduction (Ni^{3+} to Ni^{2+}), which increases the Coulomb repulsion between two e_g electrons and leads to the insulating nature.[8–10]

Since an external electric field can be applied to control the proton diffusion and induce the resistance change of *RE*NiO_3,[11,12] this guarantees that the protonated *RE*NiO_3 (H-*RE*NiO_3) materials could be good candidates in future iontronic devices, such as resistive random-access memory (ReRAMs).[13] Aside from tuning the electrical conductivity, by controlling the ionic insertion/extraction in strongly correlated oxides, thermal conductivity modulation has also emerged as another possible aspect of potential application.[14–18] Especially, by reversible protonation and deprotonation, our previous research has proved that $LaNiO_3$ and $NdNiO_3$ exhibit wide-range thermal conductivity modulations in comparison with other perovskite oxides.[19] However, these previous reports are mainly performed on high-cost single-crystal oxide ceramic substrates [e.g. $((LaAlO_3)_{0.3}$-$(SrAlTaO_3)_{0.7})$ LSAT, Yttria-Stabilized ZrO_2 (YSZ) etc.], which not only hinders the large amount of production but also lowers the device compatibility with mature silicon (Si) based semiconductor techniques.

In this work, we used buffer-layer-deposited (100) Si single-crystal wafers for epitaxial growth of $LaNiO_3$ thin films. The buffer layer is composed of Pt/ZrO_2 layers that are epitaxially grown on (100) Si. Since the in-plane lattice parameter of the Pt layer is 3.924 Å, which results in a 2.04% mismatch with $LaNiO_3$ (3.840 Å). Hence, we expected that cubic $LaNiO_3$ can be epitaxially stabilized on the (001) Pt surface. As a result, we successfully fabricated $LaNiO_3$ epitaxial films on the buffer layer-deposited (100) Si substrates and modulated the thermal conductivity by the electrochemical protonation/deprotonation technique. Our work reveals the possibility of fabricating strongly correlated material-based iontronic devices on a general silicon substrate, which may help to facilitate the realization of next-generation devices towards the "Beyond CMOS" strategy.

For $LaNiO_3$ epitaxial film growth, we used commercially available buffered Si substrates (KRYSTAL® Wafer, I-PEX Inc.) composed of (001)-oriented Pt (~150 nm)/(001)-oriented ZrO_2 (thickness: ~60 nm) buffer layers that were heteroepitaxially grown on a Si (100) substrate. $LaNiO_3$ thin films were deposited by pulsed laser deposition (PLD)[20] at a substrate temperature of 600 °C and oxygen pressure of 30 Pa. The deposition was performed by excimer ArF (wavelength: 193 nm) laser with a frequency of 7 Hz and an energy density of ~2 J cm^{-2}. Lattice parameter and crystallographic orientation of the $LaNiO_3$ films were evaluated by X-ray diffraction (XRD, SmartLab, Rigaku Co.). Cross-sectional structures of the $LaNiO_3$ films were observed using scanning electron microscopy (SEM: JSM-F10 and JSM-7610F, JEOL) at room temperature. The protonation was performed by ionic liquid gating reported elsewhere.[21–27] We used an ionic liquid of N,N-Diethyl-N-methyl-N-(2-methoxyethyl) ammonium bis (trifluoromethanesulfonyl)imide (DEME-TFSI).

The gating voltage and duration were set in the range of 2.8–3.3 V and 120 minutes at room temperature [Fig. 2(b)].

Other gating conditions out of this range may increase the possibility of insufficient phase change or sample damage (Supplementary Fig. S1). The thermal conductivity (κ) of the $LaNiO_3$ and H-$LaNiO_3$ films perpendicular to the substrate surface was measured by time-domain thermoreflectance (TDTR, NETZSCH Japan). Approximately 100 nm-thick Pt films were sputtered onto the film surface and used as the transducer for the TDTR measurements. The fitting was based on a tri-layer model as declared in Supplementary Table S1. Since the protonation-induced change of the bulk density and specific heat is relatively small,[19] the TDTR data was fitted assuming that the protons were distributed homogeneously. More detail of our κ-measurement is described in a previous paper.[28]

A cross-sectional SEM image [Fig. 1(b)] of the resultant film visualizes that ~138 nm-thick $LaNiO_3$ was successfully deposited on the buffer layer composed of ~141 nm-thick Pt/~57 nm-thick ZrO_2 grown on a Si substrate. Then, we measured an out-of-plane XRD pattern [Fig. 1(c)] of the film. Only intense 00 l diffraction peaks (l = 1, 2, and 3) of $LaNiO_3$ are clearly seen together with 00 l Pt/00 l ZrO_2/00 l Si, without any secondary phase. The out-of-plane lattice constant obtained from the XRD pattern of $LaNiO_3$ is 3.815 Å, which well agrees with the reported value (3.814 Å).[19,29] In-plane φ-scanning of {204} $LaNiO_3$ and {204} Pt [Fig. 1(d)] displays four-fold rotational symmetry with the same φ-angles that reveals heteroepitaxial growth occurred with a cube-on-cube relationship of (001)[100] $LaNiO_3$/(001)[100] Pt. These results denote that the epitaxial $LaNiO_3$ film is successfully fabricated on the buffered Si substrate.

Then we performed protonation of the $LaNiO_3$ films by room-temperature ionic liquid gating [Fig. 2(a)], where the proton is created from the surface electrical double layer that decomposes the water molecule.[21] The protonation process is monitored by in-situ XRD on the 001 $LaNiO_3$ peak, as shown in Fig. 2(b). When the gating voltage is applied, the 001 peak shifts towards the lower diffraction angle, indicating that the protonation-induced lattice expansion occurs until c = 3.868 Å. It is worth noting that after ~90 min., the 001 splits into two peaks and eventually results in two phases with c_1 = 3.912 Å and c_2 = 3.800 Å. This implies the possible phase separation during the protonation and our future work will focus on the details of these two protonated phases. However, such peak splitting is not observed in thinner samples, e.g. 60 nm sample, as shown in Fig. 2(c), implying that the peak splitting may be related to the strain effect. Since the in-plane lattice expansion due to the protonation is also possible with nickelate perovskite oxide,[30] it is assumed that in our sample, the in-plane and out-of-plane lattice expansions may simultaneously occur due to the strain relaxation, as suggested in Fig. 2(d). As shown in Fig. 2(e), the ex situ XRD patterns prove that protonation-induced structural modulation is nonvolatile. After heating the sample at 400 °C for 5 min in air for deprotonation, the diffraction peaks all recover, indicating

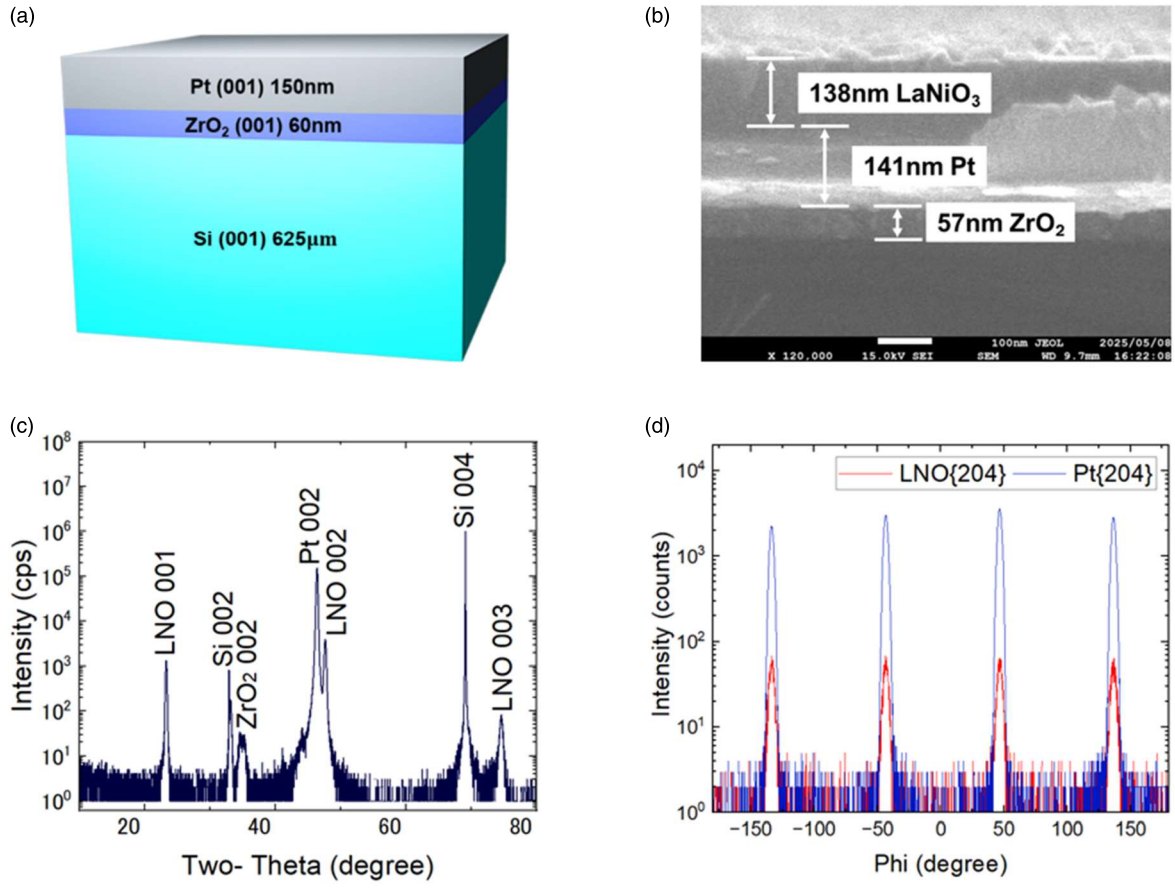

Fig. 1. $LaNiO_3$ film growth on a buffered Si substrate. (a) Schematic illustration of the buffered Si substrate. (b) Cross-sectional SEM image of a $LaNiO_3$ thin film on a buffered Si substrate. The film thickness of the $LaNiO_3$ layer is approximately 140 nm. (c) Out-of-plane XRD pattern of a $LaNiO_3$ film on a buffered Si substrate. Only intense 00 l diffraction peaks of $LaNiO_3$ are clearly observed with the diffraction peaks of the substrate. (d) In-plane XRD φ-scan of {204} $LaNiO_3$ and {204} Pt, indicating heteroepitaxial growth of $LaNiO_3$.

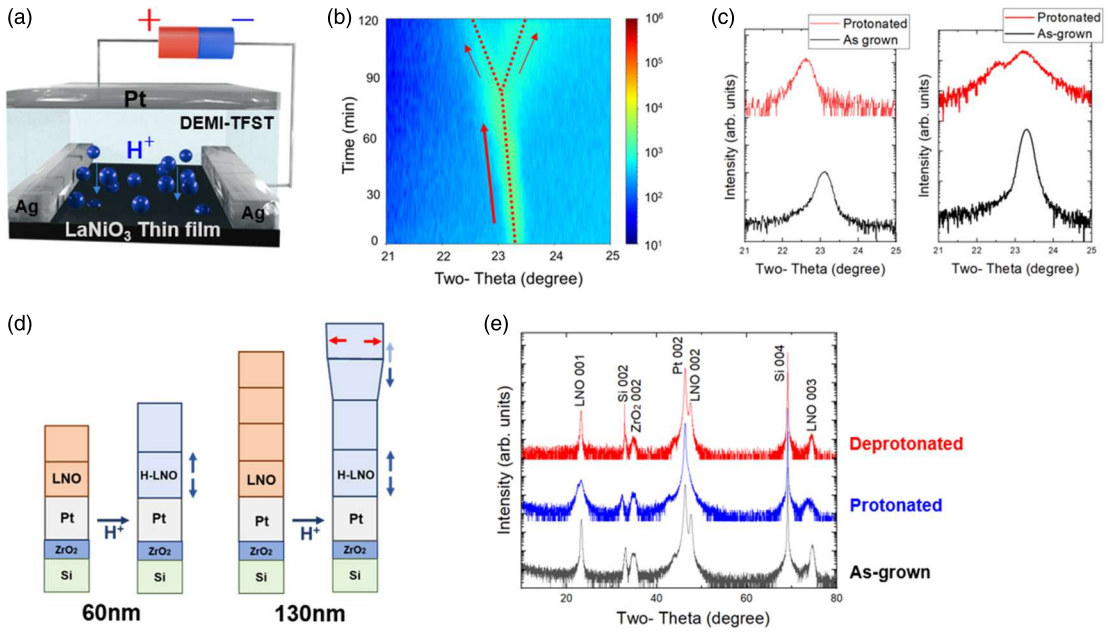

Fig. 2. Protonation/deprotonation of $LaNiO_3$ films grown on the buffered Si substrate. (a) Schematic illustration of protonation by the ionic liquid gating. (b) In-situ XRD pattern during protonation around the 001 diffraction peak of $LaNiO_3$. The peak initially shifts from 23.32° to 22.98° and subsequently splits into two peaks at 22.74° and 23.33°. (c) Out-of-plane XRD patterns around 001 $LaNiO_3$ films (left: thickness ~60 nm, right: ~130 nm) before and after protonation. The 60 nm film exhibits an overall leftward shift of the 001 $LaNiO_3$, whereas the 130 nm film shows a clear spitting into two distinct peaks. (d) Schematic representation of out-of-plane lattice expansion along the *c*-axis for the 60 nm and 130 nm $LaNiO_3$ films. This schematic highlights the difference in lattice response between the two thicknesses and illustrates a possible origin of the peak splitting observed in the thicker film. (e) Out-of-plane XRD patterns as-grown, after protonation, and after annealing. After annealing at 400 °C for 5 min (deprotonated), the peak position of $LaNiO_3$ returned to the as-grown position, confirming the recoverability of the protonated film.

the reversibility of the structural modulation in our samples. Due to the enormous leak current from the Pt layer beneath the $LaNiO_3$ thin film, the investigation of the resistivity before and after the protonation is performed on $LaNiO_3$ grown on $SrTiO_3$ (100), where the close lattice constant between $SrTiO_3$ (a = 3.905 Å) and Pt (a = 3.910 Å) guarantees the negligible strain effect. At room temperature the resistivity after protonation (Supplementary Fig. S1) is ~0.23 Ω·cm, which is ~10^3 larger than that of $LaNiO_3$ (4.0×10^{-4} Ω·cm), and this indicates that the proton concentration is about 0.4~1.0/u.c.[10)]

Finally, we measured thermal conductivity (κ) of the $LaNiO_3$ and H-$LaNiO_3$ films perpendicular to the substrate surface by the TDTR method at room temperature. Figure 3(a) shows the typical TDTR decay curve of the films. Simply, faster decay indicates higher κ. After fitting simulations of the decay curves, we obtained that the κ of the $LaNiO_3$ film (on-state) is 1.8 W m^{-1} K^{-1} and protonated $LaNiO_3$ film (H-$LaNiO_3$, off-state) is 1.0 W m^{-1} K^{-1}. Since $LaNiO_3$ exhibits Fermi liquid metallic behavior (Supplementary Fig. S2), we need to consider the electron contribution to the observed κ because observable κ is a summation of phonon contribution (κ_{lat}) and electron contribution (κ_{ele}). The reduction of κ after protonation is due to proton-insertion-governed MIT (Supplementary Fig. S2), where the κ_{ele} is greatly suppressed due to the increment of resistivity up to 3 orders of magnitude. This results in the on/off ratio of 1.8 and the switching width of 0.8 W m^{-1} K^{-1}, the thermal transistor performance is still greatly reduced compared to the previous results on LSAT single-crystal substrates [on-state: 12.0 W m^{-1} K^{-1}, off-state (protonated): 2.6 W m^{-1} K^{-1}]and YSZ single-crystal substrates [on-state: 6.0 W m^{-1} K^{-1}, off-state (reduced): 1.7 W m^{-1} K^{-1}]. By comparing the FWHM of the X-ray rocking curve of 001 $LaNiO_3$ with $LaNiO_3$ on YSZ,[28)] we found that the out-of-plane tilting of the $LaNiO_3$ crystal is large, most likely due to that of the Pt buffer layer (FWHM = 0.48°).

To further improve the κ-switching performance, rapid thermal annealing (RTA) of the substrate is performed in 10^5 Pa oxygen at 800 °C for 5 min before the thin film deposition. After depositing thin film on the RTA-treated substrate, the FWHM of the 002 Pt rocking curve decreases from 0.48° to 0.30°, consequently, the FWHM of the 002 $LaNiO_3$ rocking curve greatly decreases from 1.35° to 0.82° [Fig. 3(b)]. This helps to increase the on-state κ and eventually, the best performance on the current stage reaches 3.0 W m^{-1} K^{-1} for the on-state and 0.9 W m^{-1} K^{-1} for the off-state [Fig. 3(a)], namely on/off ratio of 3.5, comparable to that grown on YSZ. The results can be briefly quantified by the Wiedemann–Franz law $\kappa_{ele} = L{\cdot}\sigma{\cdot}T$, where L is the Lorentz number (2.44×10^{-8} W Ω K^{-2}), σ is the electrical conductivity, and T is the absolute temperature (300 K). Then, the electronic and lattice components of the $LaNiO_3$ before protonation can be calculated as κ_{ele} = 1.8 W m^{-1} K^{-1} and κ_{lat} = 1.2 W m^{-1} K^{-1}, respectively, which seemingly agrees well with the measured value. However, due to the difficulty of measuring the actual resistivity of the sample on Pt-coated silicon and the much higher thermal conductivity of $LaNiO_3$ on LSAT or YSZ, further investigation on sample resistivity and crystallinity should be necessary to pin down the fact.

In conclusion, we successfully fabricated epitaxial $LaNiO_3$ thin films on buffered Si substrates. Using RTA surface treatment before thin film deposition and operando hydrogenation, we demonstrated that the thermal conductivity can be modulated in the ranges of 0.9−3.0 W m^{-1} K^{-1}, which is

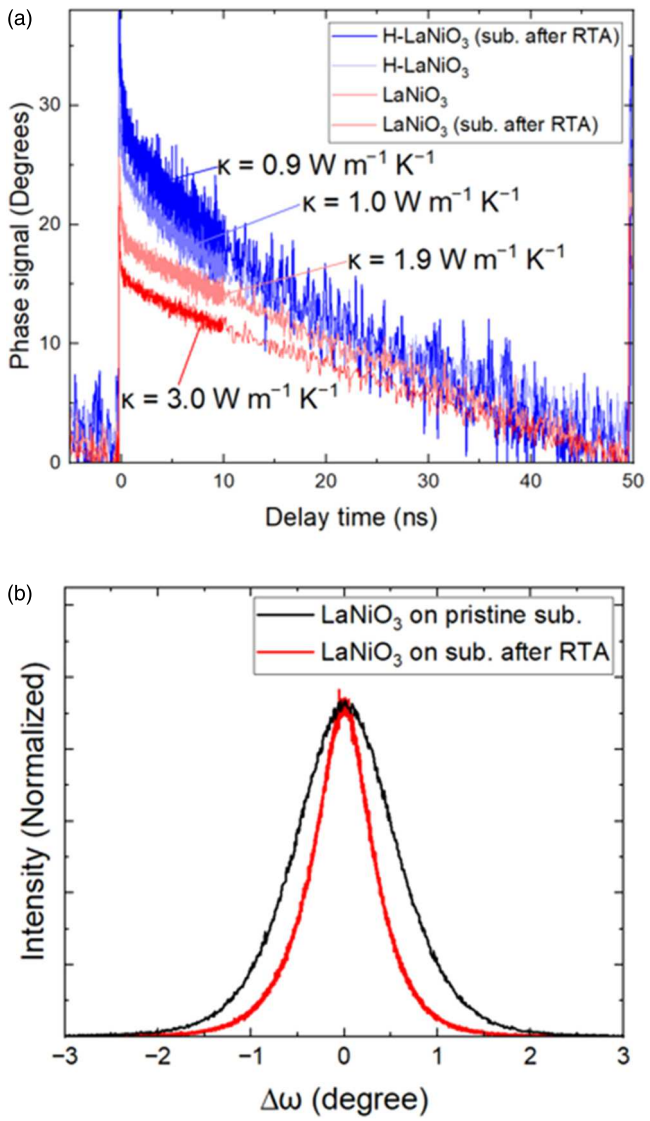

Fig. 3. Thermal conductivity versus out-of-plane crystal orientation. (a) TDTR decay curves of (H-)$LaNiO_3$ epitaxial films. In the case of the untreated Si substrate, the thermal conductivities are 1.9 W m^{-1} K^{-1} for the ON state ($LaNiO_3$) and 1.0 W m^{-1} K^{-1} for the OFF state (H-$LaNiO_3$). After depositing thin film on the RTA-treated substrate, the ON and OFF states exhibit thermal conductivities of 3.0 W m^{-1} K^{-1} and 0.9 W m^{-1} K^{-1}, respectively. These results indicate that the RTA process can effectively improve the control range of thermal conductivity. (b) X-ray rocking curves of 002 diffraction of $LaNiO_3$ films deposited on with and without RTA treatment substrate. The FWHM of the rocking curve on the RTA-treated substrate is 0.82°, narrower than that on the pristine substrate (1.3°), indicating an improvement in out-of-plane orientation. For the thermal conductivity on the RTA-treated substrate, $LaNiO_3$ and H-$LaNiO_3$ states were measured on independent samples. The FWHM of the rocking curve of the as-grown film used for protonation was 0.91°, comparable to that of the film on the RTA-treated substrate, confirming similar crystalline quality.

comparable with that of $LaNiO_3$ grown on YSZ. This work demonstrates an example to connect laboratory achievements and industrial needs, which may help to facilitate the advance of oxide electronics. In the future, further improvement of the mosaicity of the Pt buffer layer will give better performance on thermal conductivity modulation, and a wide exploration of the material grown on Si wafer.

Acknowledgments This study was financially supported by JSPS KAKENHI: Grant-in-Aid for Scientific Research (C) (25K00242). Grant-in-Aid for Specially Promoted Research (22H04914), Next Generation Young Researchers Program of the Cooperative Research Program of "Network Joint Research Center for Materials and Devices," and "Crossover Alliance to Create the Future with People, Intelligence and Materials" from MEXT. This work was also partly supported by the Advanced Research Infrastructure for Materials and Nanotechnology Open Facilities in The University of Osaka, supported by ARIM of MEXT (JPMXP1225OS1027) and by Artificial Intelligence Research Center (AIRC-SANKEN) Grant 2021. We also thank the members of the Comprehensive Analysis Center, SANEKN, The University of Osaka, for X-ray diffraction measurements. H.O. is supported by JSPS KAKENHI (22H00253).

Author declarations

Conflict of interest

The authors declare no competing financial interests.

Data availability

The datasets generated and analyzed here are available from the corresponding author upon reasonable request. Correspondence and requests for materials should be addressed to H. T. and H.-B. Li (h-tanaka@sanken.osaka-u.ac.jp, h.b.li.phys@sanken.osaka-u.ac.jp)

ORCID iDs Hao-Bo Li https://orcid.org/0000-0002-0277-0848 Hiromichi Ohta https://orcid.org/0000-0001-7013-0343

1) E. Morosan, D. Natelson, A. H. Nevidomskyy, and Q. Si, Adv. Mater. **24**, 4896 (2012).
2) W. Prellier, M. P. Singh, and P. Murugavel, J. Phys. Condens. Matter **17**, 7753 (2005).
3) H.-T. Zhang, Z. Zhang, H. Zhou, H. Tanaka, D. D. Fong, and S. Ramanathan, Adv. Phys. **4**, 1523686 (2018).
4) P. Lacorre, J. B. Torrance, J. Pannetier, A. I. Nazzal, P. W. Wang, and T. C. Huang, J. Solid State Chem. **91**, 225 (1991).
5) Y. M. Klein, M. Kozłowski, A. Linden, P. Lacorre, M. Medarde, and D. J. Gawryluk, Cryst. Growth Des. **21**, 4230 (2021).
6) W. L. Lim, E. J. Moon, J. W. Freeland, D. J. Meyers, M. Kareev, J. Chakhalian, and S. Urazhdin, Appl. Phys. Lett. **101**, 143111 (2012).
7) J. Chen et al., Appl. Phys. Lett. **107**, 031905 (2015).
8) J. Shi, Y. Zhou, and S. Ramanathan, Nat. Commun. **5**, 4860 (2014).
9) Z. Zhang et al., Nature **553**, 68 (2018).
10) I. Matsuzawa, T. Ozawa, Y. Nishiya, U. Sidik, A. N. Hattori, H. Tanaka, and K. Fukutani, Phys. Rev. Materials **7**, 085003 (2023).
11) U. Sidik, A. N. Hattori, R. Rakshit, S. Ramanathan, and H. Tanaka, ACS Appl. Mater. Interfaces **12**, 54955 (2020).
12) K. Ramadoss et al., IEEE Electron Device Lett. **39**, 1500 (2018).
13) Y. Taniguchi, H.-B. Li, K. Shimoyama, A. N. Hattori, and H. Tanaka, Appl. Phys. Lett. **122**, 263502 (2023).
14) Q. Lu, S. Huberman, H. Zhang, Q. Song, J. Wang, G. Vardar, A. Hunt, I. Waluyo, G. Chen, and B. Yildiz, Nat. Mater. **19**, 655 (2020).
15) Q. Yang et al., Adv. Func. Mater. **33**, 2214939 (2023).
16) Y. Zhang et al., Nat. Commun. **14**, 2626 (2023).
17) S. Ning, S. C. Huberman, Z. Ding, H.-H. Nahm, Y.-H. Kim, H.-S. Kim, G. Chen, and C. A. Ross, Adv. Mater. **31**, 1903738 (2019).
18) A. Jeong, M. Yoshimura, H. Kong, Z. Bian, J. Tam, B. Feng, Y. Ikuhara, T. Endo, Y. Matsuo, and H. Ohta, Science Adv. **11**, 6137 (2025).
19) H.-B. Li et al., Appl. Phys. Lett. **124**, 191901 (2024).
20) T. Yamanaka, A. N. Hattori, L. N. Pamasi, S. Takemoto, K. Hattori, H. Daimon, K. Sato, and H. Tanaka, ACS Appl. Electron. Mater. **1**, 2678 (2019).
21) N. Lu et al., Nature **546**, 124 (2017).
22) M. Wang et al., Adv. Mater. **29**, 1703628 (2017).
23) H. B. Li et al., Adv. Sci. **6**, 1901432 (2019).
24) Z. Li et al., Nat. Comm. **11**, 184 (2020).
25) M. Wang et al., Adv. Mater. **31**, 1900458 (2019).
26) D. Yi et al., Nat. Comm. **11**, 902 (2020).
27) S. Zhao, W. Hou, Z. Zhou, Y. Li, M. Zhu, H. Li, C. Li, Z. Hu, P. Yu, and M. Liu, Adv. Electron. Mater. **6**, 1900859 (2020).
28) Z. Bian, M. Yoshimura, A. Jeong, H.-B. Li, T. Endo, Y. Matsuo, Y. Magari, H. Tanaka, and H. Ohta, Adv. Sci. **11**, 2401331 (2024).
29) D. Kan, T. Hatano, A. Abe, H. Ikuta, and Y. Shimakawa, Appl. Phys. Lett. **117**, 231602 (2020).
30) U. Sidik, A. N. Hattori, K. Hattori, M. Alaydrus, I. Hamada, L. N. Pamasi, and H. Tanaka, ACS Appl. Electron. Mater. **4**, 4849 (2022).